Journal of Structural Geology, Vol. 9, No. 3, pp. 263 to 276, 1987
Printed in Great Britain

0191-8141/87 $03.00 + 0.00
Pergamon Journals Ltd.

Superposed deformations in the Eastern Alps: strain analysis and microfabrics

LOTHAR RATSCHBACHER* and GERHARD OERTEL

Department of Earth and Space Sciences, UCLA, Los Angeles 90024, U.S.A.

(*Received* 25 *February* 1986; *accepted in revised form* 31 *July* 1986)

Abstract—Superposition, mainly of two Eoalpine (Cretaceous) deformation events, can be observed in vertical sections and horizontal traverses throughout a decollement zone in the Eastern Alps consisting of crystalline basement and autochthonous and allochthonous cover stacked in several nappes. The first event is an episode with a non-coaxial strain history caused by W-directed thrusting, the second a N-directed shortening by folding and fold imbrication. Strain analysis based both on deformed pebbles and on the preferred orientation of phyllosilicate grains (March theory), microfabric analysis, and observations of the relative timing of deformation and metamorphism, together indicate that the superposition of structures caused by the two events amounts to one continuous, progressive act of deformation. We attribute gradual and consistent variations in intensity and axial ratio of the tectonic strain to a history influenced by: (a) the position of samples in the pile; (b) the relative importance of the strain increments caused by the two events; and (c) rock ductility. We interpret variations of the *c*-axis fabrics of quartz in the same way, and draw tentative kinematic conclusions for the Eoalpine orogeny in the Eastern Alps.

INTRODUCTION

MANY AUTHORS decompose a total strain into a uniaxial compactional, and a plane tectonic strain (e.g. Oertel 1970). In this article we wish to clarify for a region in the Eastern Alps the histories, in various rock units, of the superposition of two tectonic strains as a function of (a) their relative position in a pile of nappes, (b) the intensity of their overall and incremental deformation, (c) the relationship of their local to larger-scale tectonic structures and (d) their ductility histories.

First we will describe the structures caused by deformation, time the successive deformation events relative to the Eoalpine metamorphism and describe the strain in the various lithotectonic units. Second, we will correlate strain with quartz microfabrics and with large-scale structures such as folds and thrusts. With the help of these data, we will finally outline a superposition model that emphasizes the continuity of the several successive deformation events.

For the purpose of this paper, we define as 'quasi-ductile' deformations that produce a record recognizable by one or both of our two methods of strain estimation: the measurement of pebble shapes and the application of the theory of March (1932) to a series of quantitatively determined preferred orientation patterns of phyllosilicate mineral grains. All other kinds of deformation we designate as 'quasi-brittle'. Furthermore, we define as 'shear' a history of a protracted shear strain which maintains a particular family of material planes undeformed, such as bedding or foliation. As 'continuity of deformation' we designate a succession of distinct structural events connected by gradually changing parameters of a single thermal episode, a progressive strain path and overlapping rheological rock properties; the kinematic framework of the overall deformation may involve a change of principal strain axes during the successive events.

GEOLOGICAL SETTING

The study area is structurally part of the Austroalpine, the tectonically uppermost unit in the Alps. In the Eastern Alps, this large allochthonous thrust sheet is customarily subdivided into the Upper, Middle and Lower Austroalpine subunits, each of which comprises crystalline basement with a Paleozoic and/or Mesozoic cover. Of these, we are concerned only with the Middle Austroalpine unit, which includes basement and its original Permian to Mesozoic cover, and with two nappes of the Upper Austroalpine unit, the Veitsch nappe overridden by the Noric nappe. The Mesozoic section of the latter is known as the Northern Calcareous Alps (see Figs. 1 and 2).

The upper part of the Middle Austroalpine basement, which is the only part of interest here, consists of gneiss, amphibolite, ultramafic rocks and a variety of mica schists. The Permian and Mesozoic cover is up to 500 m thick and contains phyllite and quartzite, both locally pebble-bearing, and subordinate marble. The Veitsch nappe is up to 700 m thick and comprises graphite-rich metapelite to metapsammite which contain matrix-supported pebbles. An intercalated marble has been determined to be Carboniferous in age (e.g. Heritsch 1933). The Noric nappe consists of up to 3500 m of Early Paleozoic, mainly fine-grained metasediments, metavolcanics and carbonate rocks. Conglomeratic layers occur at the very base. This sequence is transgressively overlain by multicolored metasediments that constitute the base of the Northern Calcareous Alps. For recent

* Present address: Institute of Geology and Paleontology, University of Tübingen, D-7400 Tübingen, West Germany.

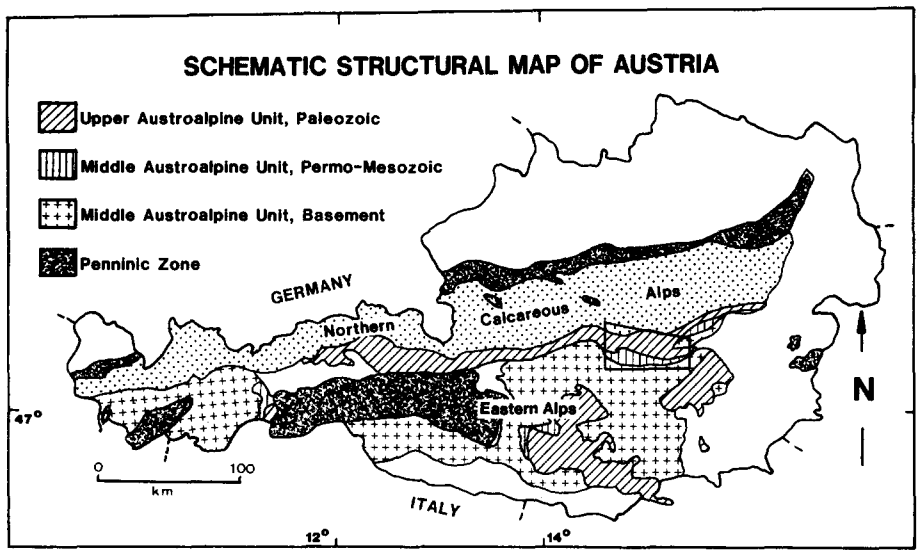

Fig. 1. Schematic structural map of the Austrian Eastern Alps with location of study area (outlined) and the political boundaries of Austria.

overviews concerning the geology of the Eastern Alps, see Tollmann (1977) and Oberhauser (1980).

Pressure and temperature were 450°C and 4–5 kbar at the base of the Permian and Mesozoic cover and 300°C and 2–3 kbar at the base of the Northern Calcareous Alps. Metamorphic conditions decreased from the hinterland toward the foreland, from S to N. The metamorphism and the related deformation reached their peak during the Cretaceous and were thus 'Eoalpine'. Metamorphic and radiometric (K/Ar method) data for the study area are from Ratschbacher & Klima (1985).

DEFORMATION STRUCTURES

Main thrusting deformation (D_1)

The principal structures of the main thrusting deformation are a foliation S_1, parallel or subparallel to the thrust boundaries and to bedding (S_0), and a NW–SE to W–E trending, generally near horizontal stretching lineation L_1 (Fig. 2). In thin-section, the foliation is marked by recrystallized primary minerals, deformed relics, metamorphic minerals and residue seams. Some moder-

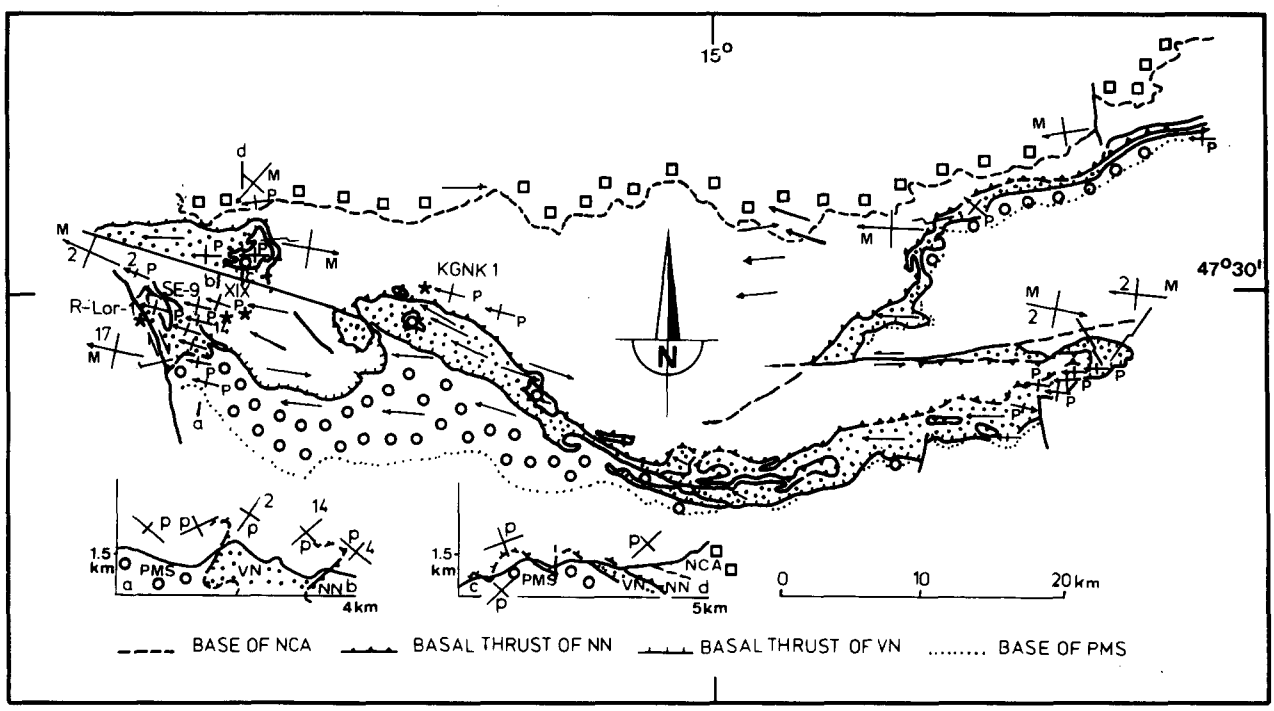

Fig. 2. Simplified structural map of the study area with cross-sections and locations of strain measurements. Stippled, Veitsch nappe; circle ornament, Permian and Mesozoic cover; square ornament, Northern Calcareous Alps. Crosses on the map, projections of XY-sections of total strain ellipsoids onto the horizontal; those on the cross-sections are projections of the XZ-sections onto the profile plane ($X > Y > Z$, principal axes). P and M, pebble and March strains. Numbers, count of specimens for each strain, where more than one was used. Arrow heads on crosses, plunge of long axes. Arrows, plunge of first Alpine stretching lineation, L_1. Asterisks, locations of quartz c-axis specimens. Thrusts, structures of the first Alpine deformation event, D_1; refolding of thrusts, structures of the second Alpine deformation event, D_2. NCA, Northern Calcareous Alps; NN, Noric nappe; VN, Veitsch nappe; PMS, Permian and Mesozoic cover.

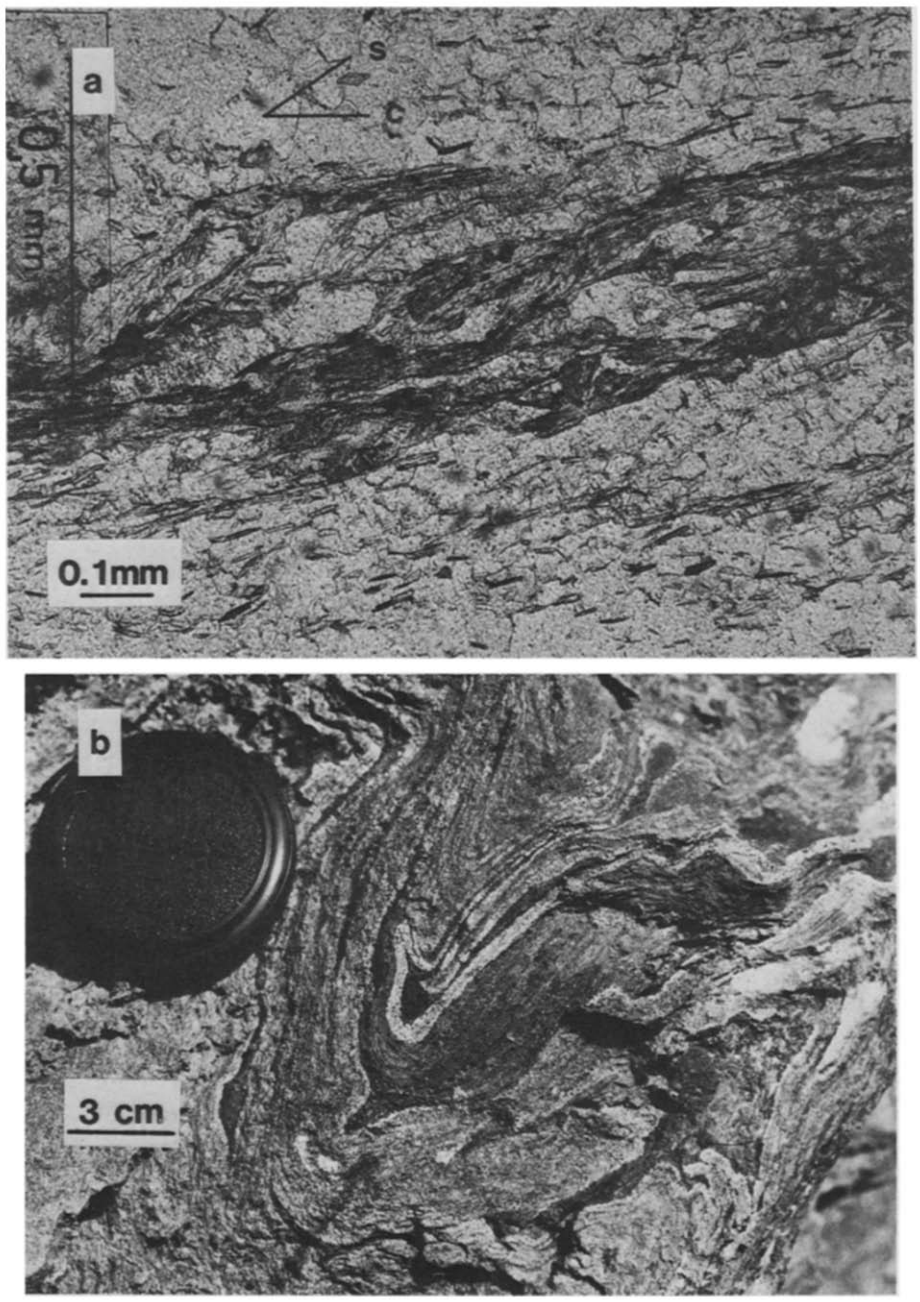

Fig. 3. (a) *S* (foliation) and *C* (shear) surfaces in quartzites of the Permian and Mesozoic cover of the Middle Austroalpine unit. (b) Profiles of Alpine folds in fine-grained, incompetent metasediments of the Noric nappe. A first fold, traced out by a Variscan quartz vein, has high limb/hinge ratio, no second-order folds, but a penetrative first axial-plane foliation. This fold is refolded by a second tight F_2 fold with significant hinge thickening and limb thinning and a 'hinge collapse', bottom left. The latter is interpreted as a result of flow of the incompetent (dark) material into the hinge during an initial flexural slip folding stage (see text).

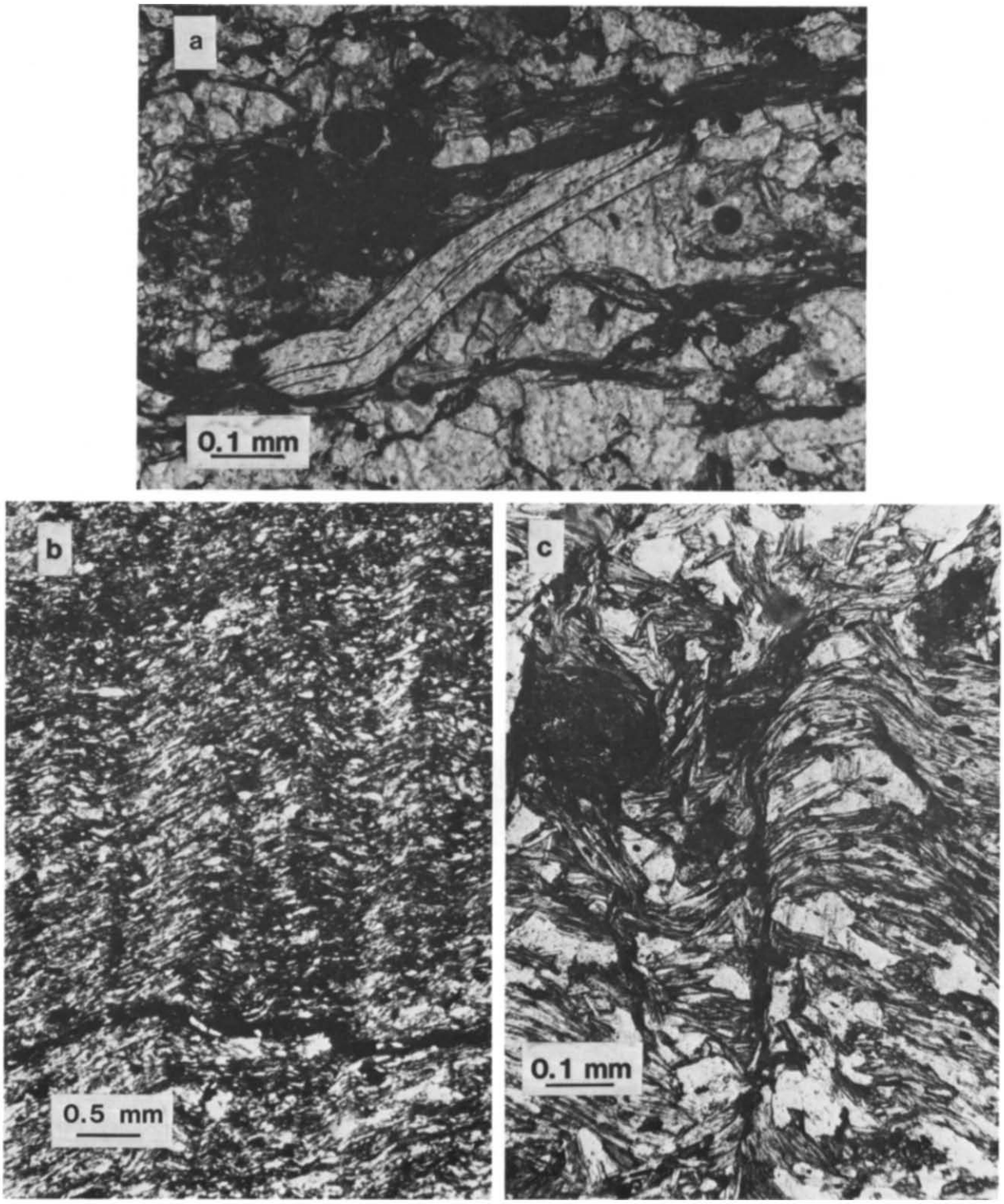

Fig. 4. Development in stages of second Alpine foliation. Foliation S_2 in metasediments of the Veitsch nappe (a) and (b) and in basement phyllonites (c). All sections perpendicular to axes of second Alpine F_2. (a) Stage of ductile shortening parallel to S_1 precedes microfolds; note microfold caused by left to right shortening at the upper right edge of a kinked detrital grain of mica. The main deformation is by flattening during the first Alpine deformation event D_1. (b) Stage of crenulation before formation of S_2, note sinusoidal microfolds; the first Alpine foliation is left to right. (c) Stage of formation of crenulation cleavage. Note solution surfaces along S_2. This stage is rarely achieved in competent pebble-bearing rocks.

ately deformed coarse-grained rocks have a two-cleavage pattern comparable to those that were described by Berthé *et al.* (1979) and interpreted as the effects of a non-coaxial deformation history: S (foliation) and C (shear) surfaces (Fig. 3a). L_1 is expressed by elongated strain shadows, aligned or pulled-apart minerals, stretched pebbles, and an area free of c-axes in quartz fabric diagrams. Spacing of S_1 decreases, and the intensity of development of S_1 and L_1 as well as strain (see below) increases gradually towards thrust boundaries, and in particular towards the decollement zone between the Middle Austroalpine and the Upper Austroalpine units.

Clastic white micas that are sigmoidally bent or microfaulted are widespread. Their (001) cleavage has acted as a slip plane. Many brittle mineral clasts are cracked or faulted, and some trails formed by their debris are curved by the rotation of clasts that shed them. Opposite-sided but generally asymmetric strain shadows are developed at the ends of some brittle mineral grains. The preferred orientation patterns of quartz c-axes in quartz pebbles, quartz veins and quartzites have monoclinic symmetry.

Based on these structural features we propose that the strain history of D_1 has been non-coaxial for at least part of the time. The features show a shear sense with the top towards the NW–W with respect to a framework provided by generally near-horizontal or gently dipping material planes.

Structures affecting thrust boundaries (D_2–D_5)

F_2 folds exist from mm to km scales, are upright, verge or are overturned to the N or NE (Fig. 2), and have axes parallel to L_1 and to the strike of the whole mountain belt. Folds in competent rocks such as quartzite and thick marble layers have interlimb angles which vary between 0 and 90° with a mean of 60°. In profile, limbs are up to 10 times longer than hinge regions irrespective of fold scale. The limbs are also long in comparison to the thickness of individual layers, which is approximately constant. Fold limbs are in general straight, and parasitic folds are rare. Hinge regions are generally complicated (Fig. 3b). Most of the textural characteristics of the F_2 folds in these competent rocks, especially the complications in the hinges, are typical of flexural slip (Hobbs *et al.* 1976) and chevron folds (Ramsay 1974). In incompetent rocks, such as phyllite, folds are in general of the shear folding type (Hobbs *et al.* 1976), asymmetric, and pass into N- to NE-directed fold-thrusts and imbricated slices.

The development of S_2, the axial-plane foliation of F_2 folds in the relatively more competent rocks, can be followed through three stages (Figs. 4a–c). There is an early one of quasi-ductile shortening parallel to S_1, another of harmonic and symmetric microfolds, and a last one, rare in competent rocks, that produced a crenulation cleavage which, in most cases, is nearly orthogonal to S_1. Crenulations get increasingly asymmetric in incompetent rocks and pass into asymmetric Gleitbretter (Ramsay 1967) along which discontinuities may occur.

Folds F_3 are found only in incompetent rocks deep in the pile, where the F_2 folds are tight to isoclinal. S_3, the third Alpine cleavage, is axial-planar to these folds but occurs only sporadically. Folds of the D_4 episode trend N–S to NE–SW, and faults D_5 trend N–S and E–W. They do not belong to the quasi-ductile strain regime and have a negligible influence on the structures. D_5 structures mainly formed during the Late Alpine (Tertiary) tectonic event.

In general D_1 becomes less affected by D_2, and structures of both episodes become less penetrative passing from S to N, that is from the hinterland toward the foreland and from deeper to shallower levels in the pile. We will illustrate these transitions in terms of strain in a later section.

Next, we discuss the geometric attributes of strain during the D_2 folding. We restrict our argument to the relatively more competent rocks, the locally pebble-bearing metasiltstones and metasandstones, because pebble markers for strain analysis exist almost exclusively in these rocks. At the time of F_2 folding, the original compositional contrast of the beds had been enhanced by metamorphic segregation along S_1. Newly formed discrete S_1 surfaces had multiplied the number of potential glide planes by creating a multilayer structure of mechanical units thinner than the original beds. This texture favored flexural slip shear on S_0 and S_1 during the buckling stage (Milnes 1971) of D_2 folding, thus minimizing pervasive shear strain within the individual layers. If there was strain due to quasi-ductile deformation in the layers themselves, it was probably due to early layer-parallel shortening before the buckling. If we accept such an interpretation of the folding mechanics, similar to that postulated by Ramsay (1974) for chevron folds, and if we assume that the cleavage S_2 in the competent beds formed at right angles to the direction of maximum D_2 shortening, then we constrain the strain increments during the early stages of D_2 to have had approximately the following geometric attributes (see Fig. 5b): the most compressive incremental strain was parallel to layering and perpendicular to the fold axis, the intermediate was parallel to the fold axis and that of greatest elongation was perpendicular to layering. At an advanced stage of folding, friction on the S_0 and S_1 glide planes may have increased, flexural slip shear on these planes could have ceased, and continuing shortening could have been by attenuation of fold limbs and eventually by some shearing on S_2 planes. We observed this in the least competent rocks where D_2 folding can be seen to be due predominantly to shear on S_2 rather than S_1 surfaces.

CRYSTALLIZATION HISTORY

During D_1, quartz recrystallized syntectonically and attained a uniform grain size of about 0.2 mm in most of the nearly monomineralic quartz pebbles of the Permian to Mesozoic cover, the Veitsch nappe, and the basal

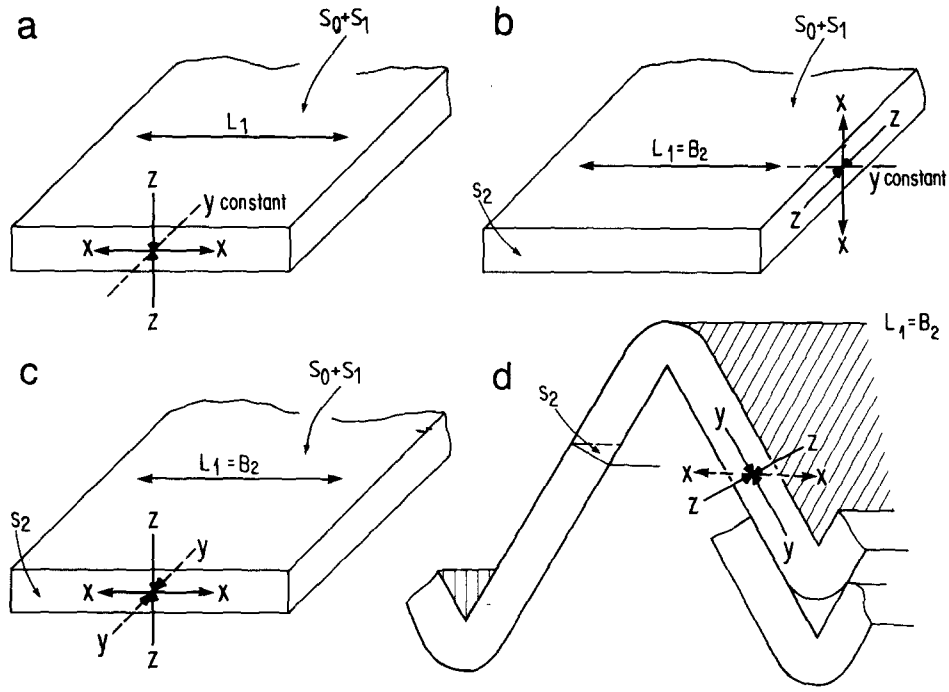

Fig. 5. Geometric attributes of strain due to quasi-ductile deformation in a single competent layer. (a) Orientation of axes after first Alpine deformation, D_1; (b) orientation of incremental strain axes during D_2; (c) orientation of cumulative strain axes after superposition of D_2 on D_1; (d) passive rotation of layers by interlayer flexural slip shear during D_2. $X > Y > Z$, principal axes of strain. While the orientation of incremental Z in (b) is fixed throughout the whole D_2 history, X and Y may be interchanged during progressive D_2 increments (see text).

parts of the Noric nappe. Phyllosilicates, mostly muscovite, biotite and chlorite, and minerals such as actinolite, epidote, quartz and calcite that recrystallized or grew during the Alpine metamorphism, are preferentially aligned parallel to S_1. In strain shadows, minerals grew as fibers parallel to S_1 and L_1. Rounded, dark, clastic tourmalines have needle-like, generally asymmetric overgrowths parallel to L_1. The ragged ends of the overgrowths interfinger with surrounding mineral grains. In most cases both overgrowths and cores are cracked, and the pieces are pulled apart. Some overgrowths include mica fibers that are aligned sub-parallel to the Alpine micas which constitute S_1 outside the overgrowths. The overgrowths must therefore have formed at the same time as the foliation. Furthermore, a few second-generation overgrowths that wrap completely around all sides of the core grains indicate a growth phase which outlasted deformation.

Mica grains parallel to S_1 were bent during D_2, and a few were kinked. Most kink-band boundaries are serrated. S_2 is marked by residue seams, and only rarely did small grains grow parallel to S_2. Mineral grains are fractured by or dissolved at their contact with discrete S_3 surfaces.

Steady-state flow, we conclude, was achieved during recrystallization of quartz in the pebbles during D_1. We also interpret growth of the main Alpine mineral assemblages to be linked to D_1. During D_2, temperatures fell but were still high enough to cause recovery of kink-band boundaries in mica. In contrast to dislocation motion, which was probably the predominant deformation mechanism in quartz during D_1, stress (pressure) solution was probably predominant during D_2. During D_3, we observe cataclastic truncation of grains in addition to their disolution, and we interpret this as evidence for a further decline of metamorphic conditions. Some metamorphic and temperature sensitive processes such as nucleation of new phases (e.g. mica, pyrite) and grain growth, however, outlasted deformation, even if probably not for long.

STRAIN

Pebble strain (Fig. 6b) was calculated by combining individual measurements with the help of a computer program described by Miller & Oertel (1979). The data plot either near the plane strain line or in the field of prolate strain. The XY-plane of tectonic strain ($X > Y > Z$ = principal strain axes; XY-plane = principal flattening plane) lies near S_1 and the X-direction near L_1. Tectonic strain intensity increases and strain becomes more prolate downward in the pile and toward the hinterland (Fig. 7c). Higher strain intensity is usually correlated with more prolate strain (Figs. 2 and 6b).

Figure 8 is a strain contour map of and cross-section through an area near the thrust between the Veitsch and overlying Noric nappes. Strain increases toward the thrust. The contoured surfaces of equal strain intensity and ratio form acute angles with the thrust. In the vicinity of the cross-section trace, mapping of sedimentological and structural features allowed identification of one large and several smaller folds in beds ranging from massive metaconglomerates through thin pebbly

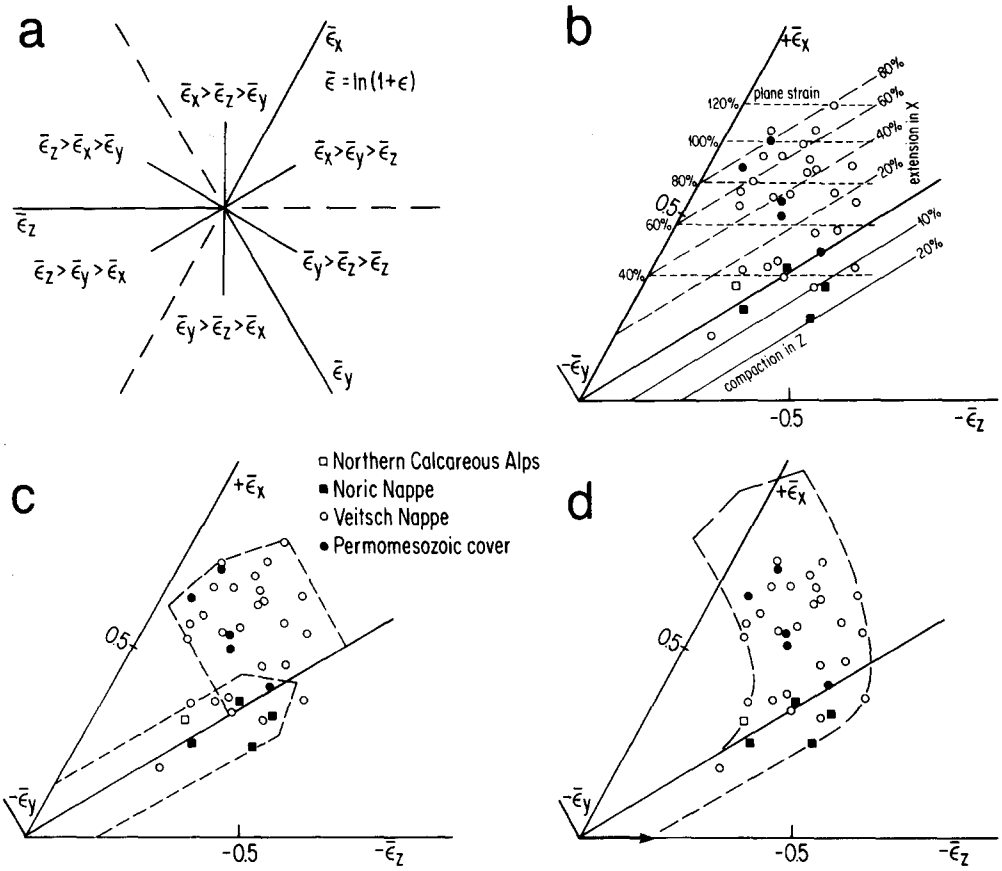

Fig. 6. Three-axes plots of natural strains measured on pebbles. (a) Axes and enclosed segments; principal natural strains (see Appendix) are $X > Y > Z$; (b) heavy line, plane strain at constant volume; inclined long-dashed lines, lines of equal volume gain or loss by extension in the X- or shortening in the Z-direction, assuming plane strain with no change of length in the Y-direction; horizontal short-dashed lines, lines of equal volume gain, assuming plane strain with no change of length in the Z-direction; (c) and (d), possible strain paths (see text).

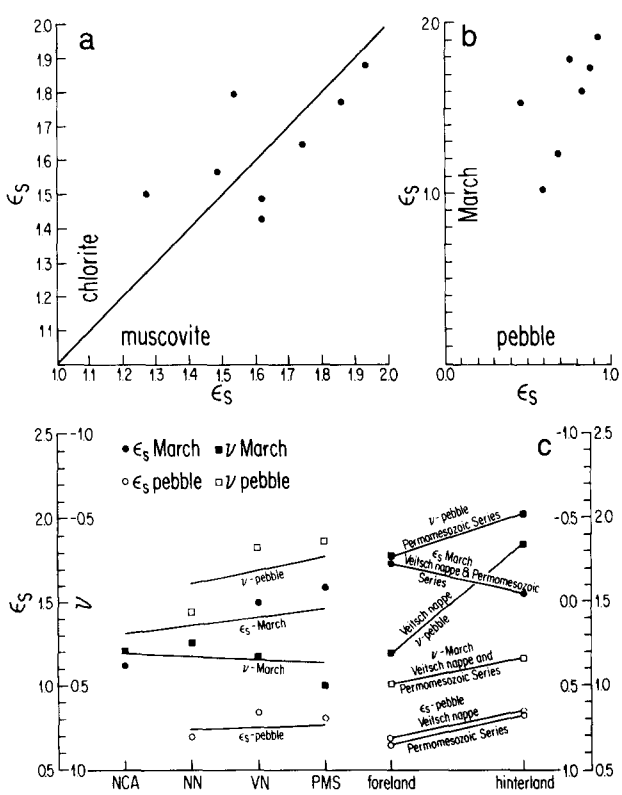

Fig. 7. Interrelations of different strain measurements. (a) Intensities of March strain (ε_s, see Appendix) calculated from chlorite versus muscovite preferred orientations measured in the same sample; the 45° line is shown for comparison. (b) Intensities of March versus pebble-shape strain, measured on the same outcrop. (c) Interrelation of intensities and ratios (ε_s and ν, see Appendix) of pebble and March strains with vertical position in the nappe pile (left) and with horizontal position between fore and hinterland (right). Labels on abscissa: NCA, Northern Calcareous Alps; NN, Noric nappe; VN, Veitsch nappe; PMS, Permian and Mesozoic cover. The foreland is to the N, the hinterland is to the S. Data points represent means of at least four samples, lines of visual best fit.

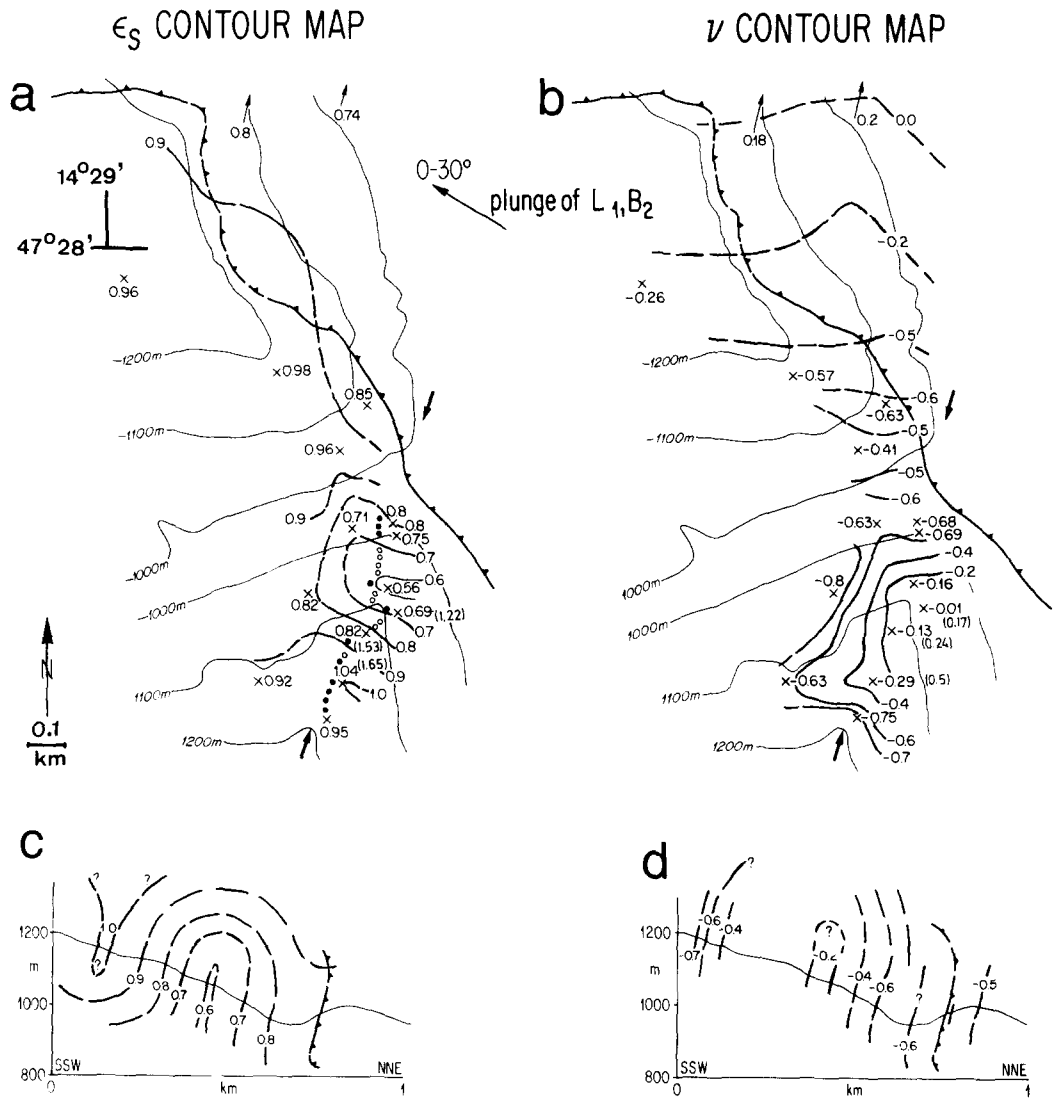

Fig. 8. Contour maps of strain intensity (a) and ratio (b) (ϵ_s, ν, see Appendix) of an area intersected by the thrust separating the Noric and Veitsch nappes. Plain numbers, pebble strain; numbers in parentheses, March strain, measured on the same outcrop. Full circles, competent, conglomeratic rock units; open circles, incompetent rock units, both shown only on (a) and only near the trace of the cross-section of (c) and (d). Thin arrows point toward data points outside the map area. (c) and (d) show hypothetical folds constructed from the systematic variation of ϵ_s and ν, respectively, along the cross-section indicated by bold-line arrows on both maps. The position of the cross-section is approximately parallel to the YZ-plane of the total strain and perpendicular to L_1 and the axes of F_2. The folds correspond approximately to real F_2 folds in the field, details of fold shape, however, have not been considered for simplicity. $X > Y > Z$, principal strain axes; L_1, elongation direction of the first Alpine deformation; B_2, fold axes of the second Alpine deformation.

metasiltstones to shales. The large fold could also be traced out by the systematic variation of the strain in samples taken along the same cross-section trace. Throughout the fold, layers with high strain intensity are usually also highly prolate. Another correlation exists between the apparent competency and the type of strain in different parts of the fold. A thin conglomeratic layer in the core, surrounded by a large volume of shales, has both the least intensive and the least prolate strain; conglomeratic layers that are either massive or have only thin shaly intercalcations are found farther from the core; they show both more intensive and more constrictional strains.

March strain samples were collected adjacent to the pebble-bearing rocks to ensure comparability with the pebble strain data. All strains lie in the flattening field (Fig. 9). Highest strain intensities are correlated with the

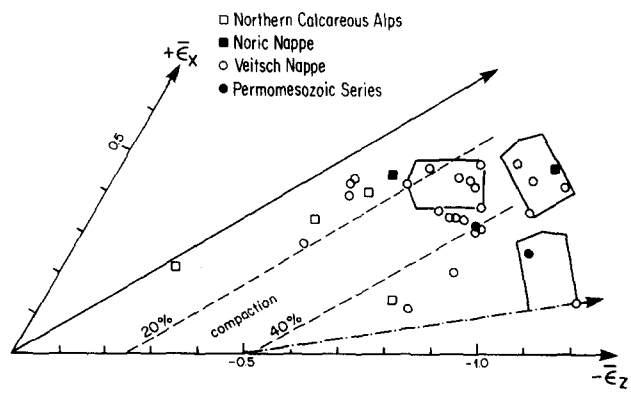

Fig. 9. Three-axis plot of March strains and the inferred strain path in incompetent rock units intercalcated between competent, pebble-bearing beds. For plot conventions, see legend to Fig. 6. Dash-dot arrow, path during D_1; Broad arrow, path during D_2. $\bar{\epsilon}_x$, $\bar{\epsilon}_y$, $\bar{\epsilon}_z$, principal natural strains, $X > Y > Z$.

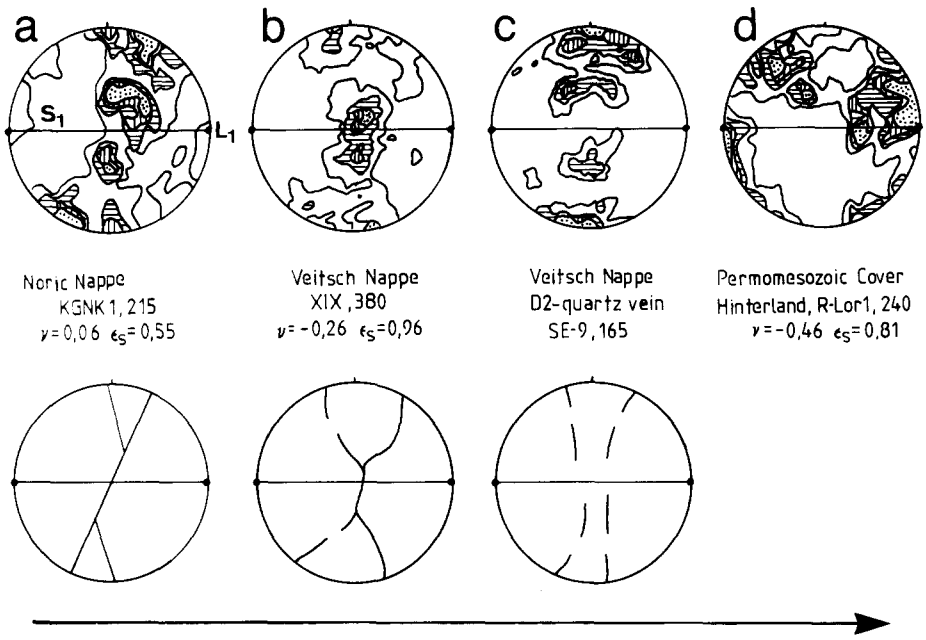

Fig. 10. Top: Quartz *c*-axis orientations; for location see Fig. 2. Equal area projection, lower hemisphere. S_1, first Alpine foliation; L_1, stretching lineation of the first Alpine deformation, D_1, which trends approximately E–W. The projection plane is the XZ-plane of total strain ($X > Y > Z$, principal strain axes). Contour intervals: 1.5, 3.5, 5.5, 7.5% per 1% area. Bottom: interpretative fabric skeletons (Lister & Williams 1979). The arrow at the bottom of the figure shows the direction of increasingly prolate total strain, of the increasing influence of the second Alpine deformation D_2 strain increments on the total strain, and of increasing pressure and temperature both during the hotter first and the cooler second phases of Alpine metamorphism. The first phase presumably left an imprint like that on (a) on all samples, but this was increasingly overprinted during the second phase in samples (b)–(d).

greatest deviations from plane strain. The principal axes of largest and intermediate March strain lie near S_1. Figures 2 and 7(c) show that data existing for the Veitsch nappe and the Permian to Mesozoic cover indicate March strain intensities increasing both with depth in the nappe pile and toward the foreland.

Where it was possible to sample the same outcrop for both pebble and March strain analysis along the cross-section trace of Fig. 8, we found that high intensities of pebble strain correlate positively with those of March strain, but that the strain ratios are inversely correlated, samples with highly prolate pebble strains have highly flattened March strains.

FABRICS

Quartz *c*-axis orientations were measured on the universal stage by Ratschbacher (1984a) for a regional analysis of fabrics. For the present study, we selected four specimens from the western edge of the area to analyse the effects of the deformation history on the development of the fabrics. The samples cover different vertical positions in the nappe pile and show more prolate strain and more highly metamorphic conditions with increasing depth. Strain measurements for these samples are based on pebble shapes.

Strain in sample KGNK1 from the base of the Noric nappe is closest to plane strain ($\nu = 0.06$, see appendix). The *c*-axis pattern from one of the quartz pebbles in this sample (Fig. 10a) possesses incomplete type I crossed girdles (Lister 1977). From the distribution of maxima along the girdles we infer that basal, rhombohedral and prismatic slip in the crystallographic *a*-direction could all have contributed to the development of this fabric (Bouchez & Pécher 1981, Schmid & Casey 1986). Specimen XIX from the uppermost part of the Veitsch nappe has a moderately prolate strain ratio ($\nu = -0.26$). Its *c*-axis fabric (Fig. 10b), again from a single quartz pebble, should probably be considered as one with incomplete type II crossed girdles (Lister 1977). Field data show that a quartz vein of another sample, SE9, also from the Veitsch nappe, must have formed late during the period of quasi-ductile deformation and thus probably during D_2. Its *c*-axis fabric (Fig. 10c) may be regarded as possessing incomplete cleft girdles (Lister & Hobbs 1980). Basal combined with rhombohedral, as opposed to prismatic, slip seems to have predominated in the development of this fabric. Quartz pebbles in specimen R-Lor1 from the Permian to Mesozoic cover sediments deepest in the pile, found just above a dolomitic limestone and a serpentinized ultramafic body in the basement, indicate a prolate strain ($\nu = -0.46$); the quartz grains of these pebbles have a diameter of about 0.8 mm, and their *c*-axis orientation pattern (Fig. 10d) differs from that of the other specimens by having pole-free areas that surround both the Z- and the Y-directions of the total strain.

The preferred orientation of the basal planes of muscovite and chlorite grains was measured with a modified X-ray pole-figure goniometer (Oertel 1970, Oertel *et al.* 1973). We determined the principal fabric intensities and their orientations by combining patterns from two orthogonal sections of the same specimen. For all but

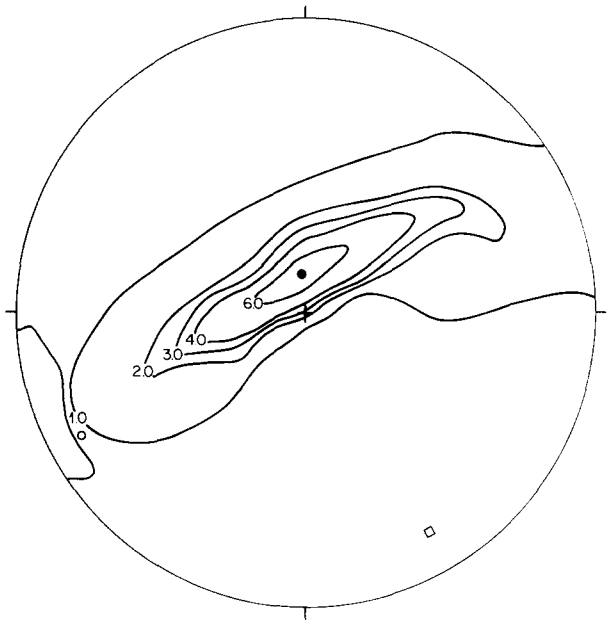

Fig. 11. Preferred orientation pattern of ehlorite basal-plane poles in specimen SE55. Equal area projection, lower hemisphere. Contours in multiples of uniform distribution. Dot and circle marks, maximum and intermediate intensities. Cross, center of projection and pole to macroscopic S_1, the first Alpine foliation. Square, least intensity and trend of stretching lineation of first Alpine deformation.

the finest-grained samples we used the translation device described by Lipshie *et al.* (1976).

All phyllosilicate pole figures show a girdle approximately normal to L_1 and thus to S_1. The maximum and minimum pole densities plot near the foliation normal and L_1, and the intermediate pole density lies nearly in the S_1 plane. The pole intensity contours of samples with weak preferred orientation show more widely spaced girdle-parallel contours on one side of the maximum than on the other (Fig. 11), and they thus deviate more from orthorhombic symmetry than do those in patterns measured in more intensely deformed rocks. In some of the specimens, the texture producing S_1 is complex and consists of S and C surfaces; these are revealed in fabric diagrams by a shift of the maximum away from the macroscopically estimated foliation normal and by asymmetric contour spacing, tighter on one side of the girdle than the other (Fig. 11). On the other hand, asymmetric contour spacing along the length of the girdle on opposite sides of the maximum is the effect of refolding S_1 by F_2 microfolds with an axial-plane foliation S_2 at an acute angle with S_1 (also observable in Fig. 11).

MODEL OF STRAIN SUPERPOSITION

Basing his argument on the D_1 structures, Ratschbacher (1983) interpreted the strain history in the decollement zone between the Middle and Upper Austroalpine units as predominantly one of simple shear. We therefore consider a plane-strain path as the most probable for this deformation event. Our interpretation of the orientation of principal strain axes during D_1 is shown in Fig. 5(a). During D_1, pervasive deformation low in the pile happened simultaneously with increasingly prominent slip on discrete surfaces by thrusting in the higher parts of the pile with lesser overburden. As a consequence, quasi-ductile D_1 strain, the only strain recorded in the rocks, varies with depth. Analogously, recorded strain decreases toward the foreland because of the lesser metamorphism and resulting shorter duration of quasi-ductile flow (Fig. 7c).

The superposition of D_2 strain increments on strain due to D_1 is nearly coaxial, however, with a changed kinematic framework (Figs. 5b & c): the Y-axis of D_1 strain acts as the most compressive incremental strain direction of D_2. Therefore, the new cumulative principal strain axes still coincide with the D_1 structures, the long axis is still approximately parallel to L_1 and the short axis to the normal of S_1 (Figs. 5c & d). The composite strain, however, is more prolate than that due to D_1 alone (Fig. 5c).

The chevron fold model of Ramsay (1974) seems to fit the F_2 folding reasonably well in the more competent rocks of the pile; we propose that layer-parallel shortening normal to L_1, along the original intermediate axis, was the initial phase of this folding event. It was followed by buckling such that there was progressively less layer-parallel shortening (Milnes 1971). Final appression of the folds was accomplished by quasi-brittle flexural slip along S_1 and S_0, which acted as shear planes. This left the strain inside each layer unaffected apart from a rigid body rotation (Fig. 5d).

Because the orientation of the initial shortening of D_2 was parallel to the Y-axis of the D_1 strain (Fig. 5b) the superposition was coaxial and resulted in a prolate total strain. During D_2, as during D_1 before, a gradient of tectonic strain must have developed in the pile. We therefore suggest that decreasing metamorphism, and thus decreasing duration of quasi-ductile rock behavior during D_2, led to strains that were less and less intensive with higher vertical position in the pile and with more northerly horizontal position toward the foreland. Plane-strain and simple-shear D_1 structures should therefore be best preserved highest in the pile and nearest the foreland.

No direct measurements are available of the strain intensity due to layer-parallel shortening alone. Theoretical and experimental studies of folding single or multi-layered materials (e.g. Biot 1961, Sherwin & Chapple 1968, Hudleston 1973, Hudleston & Stephansson 1973, Ramsay 1967, 1974) indicate that early layer-parallel shortening plays an important role where the viscosity contrast between layers is moderate (i.e. $\ll$1000). In our case, this contrast was probably enhanced by metamorphic differentiation and by the selective formation of S_1 cleavage in those protoliths that were already the least competent to begin with. Contrasts may have exceeded the range between 14 and 30 that was measured by Sherwin & Chapple (1968) on quartz veins in a phyllitic matrix. Up to 30% layer-parallel shortening during D_2 therefore appears to be a possible first-approximation estimate. Shortening up to 33% was estimated by Fischer & Coward (1982) in quartzitic layers of the Moine Thrust Zone in Scotland.

DISCUSSION

Pebble strains and quartz microfabrics

The computer program described by Miller & Oertel (1979) finds strain statistically under the assumption that pebbles were initially oriented at random. The validity of this assumption is uncertain, but test comparisons with the R_f/ϕ method of Dunnet (1969) and Peach & Lisle (1979), the shape-factor-grid method of Elliott (1970) and the 'X-ROT' program of Matthews *et al.* (1974) gave no indication to the contrary; within the margins of observational uncertainties, the assumption of original randomness was not invalidated by any of these methods. For the pebbly rocks of the Veitsch nappe it can be independently inferred from sedimentological evidence that they were deposited as debris flows (Ratschbacher 1984b); poorly developed, nearly random clast fabrics are considered typical for this type of sediment (Nardin *et al.* 1979). Initial axial ratios, determined by several of the unstraining methods mentioned above, seem to have been near 1.3/1.3/1 for most samples. This pretectonic preferred alignment of the two longer pebble axes was found to lie in the bedding plane and taken to be due to up to 23% of bedding-normal compaction.

The effect of the superposition of strain increments that seems most probable to us is schematically shown in Fig. 6(c). Pre-tectonic compaction may have flattened the sediment from very little up to 15%. We derive this estimate from the scatter of all the low-intensity data. The first tectonic event is depicted by the dashed wide arrow parallel to the plane-strain line. The arrow width is due to the compaction scatter. The length of this first arrow corresponds to a path of plane strain mostly due to D_1. This path is taken to have gone as far as the most intensive strains observed near the plane-strain line.

The second deformation D_2 can be represented, we think, by the broad arrow orthogonal to the plane-strain line in Fig. 6(c). It points in the negative Y-direction and encompasses all the most intensive strains and those differing significantly from plane strain. Variations in the intensity of the second strain are mainly due to the effect of sample position in different parts of the nappe pile, the top and north of which are little affected by D_2 (Fig. 7c).

Strain variations in the area of Fig. 8 we interpret in the following three ways. (a) The thrust surface is accompanied by a zone of intensive strain. (b) Both overall strain intensity and that of the superposed D_2 strain alone are influenced by rock competency and bed thickness. Incompetent domains are strained preferentially, thus lowering the strain intensity in thin, intercalated, pebble-rich layers. This is most apparent in the core of the fold shown in cross-section in Fig. 8, where a thin, pebbly bed between thick shales is remarkably little deformed. Such beds may have buckled earlier than others, thus undergoing less quasi-ductile layer-parallel shortening than equally competent but more massive beds. (c) Non-parallelism with the thrust of the surfaces of equal strain intensity or ratio may also partly be due to the inhomogeneity of strain from D_1 in addition to that from D_2.

In conclusion, D_2 intensified the D_1 strain only slightly, but it caused the cumulative strain to change from plane to constrictional. The intermediate cumulative strain, parallel to the direction of greatest D_2 compression, did not exceed 26% shortening and thus differs little from the 33% quasi-ductile layer-parallel shortening to be expected at the early stages of the second folding.

We base an interpretation of quartz c-axis fabrics on a combination of conclusions from earlier observations in natural rocks (e.g. Bouchez 1977, Brunel 1980, Bouchez & Pécher 1981, Behrmann & Platt 1982, Schmid & Casey 1986) with those from the computer simulations by Etchecopar (1977), Lister *et al.* (1978), Lister & Williams (1979) and Lister & Hobbs (1980). Type I crossed-girdle patterns are, according to these investigations, most commonly found in quartz tectonites that have been subjected to a history of plane strain. The inclination of the fabric 'skeleton' (Lister & Williams 1979) of specimen KGNK1 points to a rotational component in its deformation history. We interpret this fabric as representing on the whole only the simple shear of D_1 when the rock moved to the NW or W, approximately parallel to L_1. This interpretation fits with the tectonically high position of this sample, with its proximity to the foreland and with the measurement in it of a plane strain.

The other three fabrics shown in Fig. 10(b)–(d) provide, we suggest, evidence for (a) an increasing modification by the D_2 episode of what we assume to have formerly been D_1 fabrics toward ones fitting a prolate strain, (b) a decrease of metamorphic temperatures during the time from the end of D_1 to that of D_2, and (c) an influence of fluid activity and temperature on the preferred orientation patterns of quartz c-axes.

The transition from type I crossed girdles, as in sample KGNK1, to the type II crossed and cleft girdles in sample XIX and SE9, corresponds to increasingly prolate total strains caused by the greater influence of D_2 (Fig. 10). It may also, in accordance with similar observations by Bouchez (1977), Lister & Hobbs (1980) and Schmid & Casey (1986), indicate an effect that the deformation history had on the quartz fabrics, a history which in our case went from plane to constrictional. The apparent predominance of basal glide in producing the fabric of sample SE9 indicates a temperature during deformation lower than that for samples KGNK1 and XIX; in those, rhombohedral and prismatic glide seem to have contributed as well (Baëta & Ashbee 1969, Tullis *et al.* 1973, Bouchez 1977, Bouchez & Pécher 1981, Schmid & Casey 1986). We regard this as a confirmation for the temperature history we propose. The microfabric of sample R-Lor1, we further suggest, shows the strongest influence of D_2. Its position deep in the pile at a high temperature at the time of D_2, and with high fluid activities caused by the serpentinization of nearby ultramafic rocks, favored recrystallization, grain-growth

and rearranging of the hypothetical previous preferred orientation of *c*-axes caused by D_1.

Assuming that axis-free areas in fabric diagrams correspond to directions of greatest total extension, as is commonly observed in deformed quartzites, we conclude that in the lowermost part of the pile the direction of greatest extension plunges to the S. The microfabric of sample R-Lor1 thus fits the same strain increment that is revealed in the incompetent rocks deep in the pile in which the S_2 foliation transects tight F_2 folds. There, S_2 surfaces dip at various angles toward the south, and asymmetric crenulations suggest relatively northward shearing of the higher over the lower domains. During that part of the strain history the direction of greatest extension lay everywhere, as it does in sample R-Lor1, in a nearly vertical N–S plane.

At constant volume, and with the strain history remaining coaxial at the transition from D_1 to D_2, an episode of shortening in the direction of the formerly intermediate strain must have been compensated for by stretching along either one or both of the remaining axes. We suggest that maximum extension during the early stages of D_2 continued in the same direction as before. This seems to be indicated by our interpretations of two facts: (a) strain intensity can only increase beyond what it was at the end of D_1 if the further strain path provides additional extension in the previous direction of greatest elongation; and (b) the quartz fabrics have independent features indicative of increasing extension along the same direction as before, and increasingly so in samples in which the D_2 strain seems larger. During the latest stages of the superposed deformation, however, the direction of greatest incremental extension appears to have switched to the direction of the former intermediate strain.

Figure 6(d) shows what we consider the most probable deformation path: plane strain with no change in Y was followed by axially symmetric extension along X, then a different plane strain produced no change in Z and, finally, axially symmetric shortening had its unique axis along Y. We consider the whole strain history as one of continuous progressive deformation.

March strains and phyllosilicate pole figures

According to the method described by Oertel & Curtis (1972) and Lipshie *et al.* (1976), we calculated 'March strains' from the maximum, intermediate and minimum intensities of muscovite and chlorite pole figures assuming no volume change. Where necessary to allow such calculation, we imposed orthorhombic symmetry on the pole figures. Previous studies (e.g. Oertel 1970, Etheridge & Oertel 1979, Rumble & Oertel 1979) critically assess the applicability of the March method in highly deformed rocks. These studies have shown that deviations from orthorhombic symmetry in the orientation patterns of phyllosilicates, which are impermissible according to the March theory, may be caused by growth of new mineral grains, by coarsening of pre-existing grains, by inhomogeneous nucleation, by diffusive processes during deformation, or by complex domainal microstructures on a scale that brings several domains into the region illuminated by the X-ray beam.

In our rocks, we suspect the growth of new minerals in strain shadows behind rigid inclusions, and from this we infer a role for diffusive processes; similarly, from the observed presence of residue seams along contacts between phyllosilicate and other grains such as quartz, feldspar, or calcite, we conclude that stress solution must have been one of the active deformation mechanisms. The observed growth of single mineral phases, say quartz, calcite, or chlorite, in strain shadows and the apparent removal of the same phases along foliation planes may indicate nucleation or growth in response to local inhomogeneities of the stress field. The appearance of new phases, coarsening of pre-existing grains, and local dissolution, nucleation and growth, however, should have affected chlorite and muscovite differently because of their unequal sensitivity to changes in chemical and thermal conditions. In eight samples we determined the preferred orientation of both phases and found that the calculated strains do not differ systematically (Fig. 7a). Although various processes that can disturb March preferred orientations of phyllosilicates were certainly active in our rocks, they did not, we conclude, modify them to such a degree that they could not be of semiquantitative use. We are, however, aware that mechanisms of grain orientation other than rigid rotation could have falsified the strains calculated from the preferred orientation patterns, and we therefore designate them formally as 'March strains'.

Samples in which S_1 is almost unaffected by later crenulations show the most intensive preferred orientations, with up to 37 times uniform density at the maximum. Preferred orientations of this type are probably responsible for the ease of gliding on S_1 during early increments of D_2 and therefore for slip between phyllosilicate grains rather than their further rotation. It is uncertain to what degree this mechanism could falsify March strains and cause an incomplete recording of the D_2 component; we will disregard this possibility.

In Fig. 7(b) we compare March strain intensities with those estimated by measuring pebble shapes; they agree reasonably well. Samples for both methods were taken from the same outcrops and at the least possible distance from each other. The two kinds of strain also agree well in the orientation of their principal axes; they fit least well in the proportions of their principal strains; of these, the mean maximum elongations fit most closely (+83% and +117% for the pebble and March strains, respectively). The mean least (−39% and −69%) and intermediate strains (−10% and +25%) show that flattening normal to S_1 is accompanied mainly by elongation along the stretching axis in the pebbles, whereas elongation in the phyllosilicate-rich rocks is more evenly distributed in the foliation plane. Neither pebble nor March strains, we conclude, provide an exact estimate of the total rock strain. As 'total strain' we designate here one that comprises the shortening normal to bedding during sediment compaction (Oertel & Curtis 1972) as well as

the tectonic strain. The pebble strains may approximate the tectonic strain of the relatively competent portions of the pile, in contrast to the generally incompetent phyllosilicate-rich rocks that are amenable to March strain measurements. Stronger compaction may partly account for the more pronounced flattening generally registered by the March analysis. Another difference in the response to tectonic stress may have been greater volume loss by solution of the phyllosilicate-rich rocks. The difference in strain intensity may thus record different rheological behavior during deformation as well as sediment compaction.

We interpret the high intensities and strong flattening in the foreland portion of the deep nappes registered by March strain as the combined effects of pre-tectonic compaction and tectonic strain accompanied by volume loss during D_1. The locally differing added effect of D_2, varying with position in the pile, is reflected by its effect on the phyllosilicate fabrics. At the top, in the Northern Calcareous Alps, shortening by D_2 acted on a rock with a weak S_1 which therefore hardly affected the orientation of the D_2 strain. Deviations from coaxial superposition were therefore marked and caused a somewhat asymmetric crenulation or microfolding, with the new cleavage and axial planes deviating from the normal to S_1. These folds thus cause total preferred orientation patterns with a symmetry lower than orthorhombic.

In contrast, the orientation of the D_2 strain deep in the pile is well constrained by a sharpiy developed S_1, and the superposition is forced to be almost perfectly coaxial. Early D_2 increments seem to have produced slip of phyllosilicate grains along S_1, later on their rotation, then sinusoidal microfolds, and finally S_2 planes almost perpendicular to S_1. Grain rotation, either individually or together with that of the whole limbs, but in both cases away from S_1 and into S_2 cleavage planes, weakened the intensity of preferred orientation from what it had been after D_1. The D_2 structures are symmetric with regard to S_1 and thus preserve the orthorhombic symmetry of the earlier preferred orientation patterns, and the rotation axes of the phyllosilicate grains during D_2 are parallel to the maximum elongation direction of the old strain. The result is a weakening of the girdle perpendicular to the old maximum elongation direction. This indicates reduced strain intensities and less flattening in samples in which a strong D_2 was superposed on D_1.

The effect of rock competency on the intensities of the cumulative and the superposed D_2 strain, as documented by pebble analysis in the area shown in Fig. 8, is confirmed by the March estimates in the same area. The incompetent core rocks of the large fold in the cross-section (Fig. 8) must have been strongly affected by D_2, and March strain in the one sample from this core is weak and close to plane strain. Two samples of more competent rocks in the same fold show only minor effects of strain reduction by D_2, and they therefore preserve more nearly perfectly the old strains with their pronounced flattening (Figs. 8a & b).

Figure 9 outlines the effects of strain superposition in terms of a March strain path. A tectonic strain D_1, accompanied by syntectonic volume loss, is added to a variable compactional strain. The further tectonic strain D_2 moves the cumulative strain along the wide arrow toward the plane-strain line. The intensity of the March D_2 strain depends on position in the pile in a way that is consistent with the pebble strains (Fig. 7c). Figure 9 also indicates that the March method records preferentially both the early, pretectonic compaction stage and the relatively late tectonic stages of the strain history; the D_1 portion of the strain path is only weakly defined, and strain intensities and ratios for this part of the path differ greatly between samples deformed solely by D_1 and those deformed by both D_1 and D_2.

Continuity between deformation events D_1 and D_2 is independently indicated by the crystallization and strain histories and by the quartz fabric evolution. We therefore suggest that the structures described in this paper result from one continuous progressive deformation with changing principal strain directions. Principal compression was first E–W (D_1), then N–S (D_2 and D_3) and finally again E–W (D_4). This is inconsistent with the opinion, current among students of the Eastern Alps, of a single S–N compressional episode during Eoalpine time.

CONCLUSIONS

The structural features on scales from macroscopic to microscopic that were produced by a first tectonic deformation indicate a history of plane strain combined with more or less rotation and thus ranging from pure to simple shear. In this process, a foliation formed which intensified the primary layering and created numerous new potential glide planes. The resulting anisotropy favored flexural slip and chevron folds during the second deformation, and these folding mechanisms governed the strain history from then on.

Pebble shapes portray principally the plane strain of the first deformation event, but they are increasingly prolate with depth and proximity to the hinterland. This variation in the type of strain is the consequence of differences in metamorphic temperature during the second deformation and of the locally different rheological properties this imparted to the rocks.

March strains best preserve the effects of the pre-tectonic compaction and of volume loss during tectonic deformation. The strongest preferred orientations are encountered deepest in the pile and nearest the foreland. There, they represent the almost undisturbed strain due to the first deformation alone. The intensity of the cumulative strain was progressively weakened by strain reduction during the second deformation, most markedly deep in the pile near the hinterland.

On the whole, strain paths found in different rock types and by different techniques of strain measurement are rather similar. The March method, however, is most sensitive to the late stages of the tectonic strain history and the method of strain determination by pebble shape

to its early stages. A combined analysis of strain measured by different techniques, of quartz and phyllosilicate fabrics, of crystallization histories and of field structures allow us to trace in time and space a continuous but changing deformation path. What in the field appear to be superposed structures we recognize as the record of a single, uninterrupted although complex phase of deformation. The Cretaceous Eoalpine tectonic history of a pile of Austroalpine nappes thus provides an example for a progressive deformation which began with compression along a line from east to west, continued with one from north to south, and, most probably, ended by reverting to one from east to west.

Acknowledgements—This article was prepared while L.R. was a postdoctoral scholar at UCLA when he was on leave from the Institute of Geology, Graz University, Austria. We thank P. Choukroune (Rennes), K. Stattegger (Graz), J. P. Platt as corresponding editor, and the referees for improving the manuscript. L.R. was financially supported by the Austrian Science Foundation (P5251) and received travel grants from the Fulbright Foundation and the Styrian Government.

REFERENCES

Baëta, R. D. & Ashbee, K. H. G. 1969. Slip systems in quartz: I. Experiments. *Am. Miner.* **54**, 1551–1573.

Behrmann, J. H. & Platt, J. P. 1982. Sense of nappe emplacement from quartz *c*-axis fabrics: an example from the Betic Cordilleras (Spain). *Earth Planet. Sci. Lett.* **59**, 208–215.

Berthé, D., Choukroune, P. & Jegouzo, P. 1979. Orthogneiss, mylonite and non-coaxial deformation of granites: the example of the South Armorican Shear Zone. *J. Struct. Geol.* **1**, 31–42.

Biot, M. A. 1961. Theory of folding of stratified viscoelastic media and its implications in tectonics and orogenesis. *Bull. geol. Soc. Am.* **72**, 1595–1650.

Bouchez, J.-L. 1977. Plastic deformation of quartzites at low temperature in an area of natural strain gradient. *Tectonophysics* **39**, 25–50.

Bouchez, J.-L. & Pécher, A. 1981. The Himalayan main thrust pile and its quartz-rich tectonites in central Nepal. *Tectonophysics* **78**, 23–50.

Brunel, M. 1980. Quartz fabrics in shear zone mylonites: evidence for a major imprint due to late strain increments. *Tectonophysics* **64**, T33–T44.

Dunnet, D. 1969. A technique of finite strain analysis using elliptical particles. *Tectonophysics* **7**, 117–137.

Elliott, D. 1970. Determination of finite strain and initial shape from deformed elliptical objects. *Bull. geol. Soc. Am.* **81**, 2221–2236.

Etchecopar, A. 1977. A plane kinematic model of progressive deformation in a polycrystalline aggregate. *Tectonophysics* **39**, 121–142.

Etheridge, M. A. & Oertel, G. 1979. Strain measurement from phyllosilicate preferred orientation—a precautionary note. *Tectonophysics* **60**, 107–120.

Fischer, M. W. & Coward, M. P. 1982. Strain and folds within thrust sheets: an analysis of the Heilam sheet, northwest Scotland. *Tectonophysics* **88**, 291–312.

Heritsch, F. 1933. Unterkarbone Korallen aus dem Sunk bei Trieben (Grauwackenzone von Obersteiermark). *Mitt. naturw. Ver. Steierm.* **70**, 76–82.

Hobbs, B. E., Means, W. B. & Williams, P. F. 1976. *An Outline of Structural Geology*. Wiley, New York.

Hudleston, P. J. 1973. Fold morphology and some geometrical implications of theories of fold development. *Tectonophysics* **16**, 1–46.

Hudleston, P. J. & Stephansson, O. 1973. Layer shortening and fold-shape development in the buckling of single layers. *Tectonophysics* **17**, 299–321.

Lipshie, S. R., Oertel, G. & Christie, J. M. 1976. Measurement of preferred orientation of phyllosilicates in schists. *Tectonophysics* **39**, 91–99.

Lister, G. S. 1977. Discussion: Crossed-girdle *c*-axis fabrics in quartzites plastically deformed by plane strain and progressive simple shear. *Tectonophysics* **39**, 51–54.

Lister, G. S. & Hobbs, B. E. 1980. The simulation of fabric development in plastic deformation and its application to quartzite: the influence of deformation history. *J. Struct. Geol.* **2**, 355–370.

Lister, G. S., Paterson, M. S. & Hobbs, B. E. 1978. The simulation of fabric development in plastic deformation and its application to quartzite: the model. *Tectonophysics* **45**, 107–158.

Lister, G. S. & Williams, P. F. 1979. Fabric development in shear zones: theoretical controls and observed phenomena. *J. Struct. Geol.* **1**, 283–297.

March, A. 1932. Mathematische Theorie der Regelung nach der Korngestalt bei affiner Deformation. *Z. Kristallogr.* **81**, 285–297.

Matthews, P. E., Bond, R. A. B. & Van den Berg, J. J. 1974. An algebraic method of strain analysis using elliptical markers. *Tectonophysics* **24**, 31–67.

Miller, D. M. & Oertel, G. 1979. Strain determination from the measurement of pebble shapes: a modification. *Tectonophysics* **55**, T11–T13.

Milnes, A. G. 1971. A model for analysing the strain history of folded competent layers in deeper parts of orogenic belts. *Eclog. geol. Helv.* **64**, 335–348.

Nardin, T. R., Hein, F. J., Gorsline, D. S. & Edwards, B. D. 1979. A review of mass movement processes, sediment and acoustic characteristics, and contrasts in slope and base-of-slope systems versus canyon–fan–basin floor systems. *Spec. Publ. Soc. econ. Palaeont. Miner., Tulsa* **27**, 61–73.

Oberhauser, R. 1980. *Der geologische Aufbau Österreichs*. Springer, Wien.

Oertel, G. 1970. Deformation of slaty, lapilli tuff in the Lake District, England. *Bull. geol. Soc. Am.* **81**, 1173–1180.

Oertel, G. & Curtis, C. D. 1972. Clay–ironstone concretion preserving fabrics due to progressive compaction. *Bull. geol. Soc. Am.* **83**, 2597–2606.

Oertel, G., Curtis, C. D. & Phakey, P. P. 1973. A transmission electron microscope and X-ray diffraction study of muscovite and chlorite. *Mineralog. Mag.* **39**, 176–188.

Peach, C. J. & Lisle, R. J. 1979. A FORTRAN IV program for the analysis of tectonic strain using deformed elliptical markers. *Comput. Geosci.* **5**, 325–334.

Ramsay, J. G. 1967. *Folding and Fracturing of Rocks*. McGraw-Hill, New York.

Ramsay, J. G. 1974. Development of chevron folds. *Bull. geol. Soc. Am.* **85**, 1741–1754.

Ratschbacher, L. 1983. Ein Modell zur alpidischen Deckgebirgsdeformation im Ostabschnitt der Ostalpen basierend auf einer vollständigen Gefügeanalyse: ein Vorbericht. Anzeiger österreichische Akademie der Wissenschaften, mathematische-naturwissenschaftliche Klasse 1983, 69–73.

Ratschbacher, L. 1984a. Kinematische Analyse der Deckenbewegungen und assoziierter Deformation im Deckgebirge der östlichen Ostalpen (Obersteiermark, Österreich). Jahresbericht 1983 österreichischer Hochschulschwerpunkt S 15, Graz, 67–200.

Ratschbacher, L. 1984b. Beitrag zur Neugliederung der Veitscher Decke (Grauwackenzone) in ihrem Westabschnitt (Obersteiermark, Österreich). *Jb. geol. Bundesanst, Wien* **127**, 423–453.

Ratschbacher, L. & Klima, K. 1985. Übersicht über Gesteinsbestand und Metamorphose in einem Querprofil vom Altkristallin zur Kalkalpenbasis (Österreich). *Jb. geol. Bundesanst., Wien* **128**, 151–173.

Rumble, D. & Oertel, G. 1979. Strain and metamorphism: metaclastic rocks from New Hampshire. *J. Geol.* **87**, 69–86.

Schmid, S. M. & Casey, M. 1986. Complete fabric analysis of some commonly observed quartz *c*-axis patterns. In: *Mineral and Rock Deformation: Laboratory Studies—The Paterson Volume, Geophysical Monograph* **36**, 263–286.

Sherwin, J. A. & Chapple, W. M. 1968. Wavelengths of single layer folds: a comparison between theory and observation. *Am. J. Sci.* **266**, 167–179.

Tollmann, A. 1977. *Geologie von Österreich. Die Zentralalpen*. Franz Deuticke, Wien.

Tullis, J., Christie, J. M. & Griggs, D. T. 1973. Microstructures and preferred orientations of experimentally deformed quartzites. *Bull. geol. Soc. Am.* **84**, 297–314.

APPENDIX

Strain intensity, ε_s, is here defined as:

$$\varepsilon_s = \frac{\sqrt{3}}{3}\left[(\bar{\varepsilon}_1 - \bar{\varepsilon}_2)^2 + (\bar{\varepsilon}_2 - \bar{\varepsilon}_3)^2 + (\bar{\varepsilon}_3 - \bar{\varepsilon}_1)^2\right]^{1/2},$$

and strain ratio, ν, as:

$$\nu = (2\bar{\varepsilon}_2 - \bar{\varepsilon}_1 - \bar{\varepsilon}_3)/(\bar{\varepsilon}_1 - \bar{\varepsilon}_3),$$

where $\bar{\varepsilon}_i = \ln(1 + \varepsilon_i)$ is a principal natural strain corresponding to ε_i, its conventional counterpart (Hobbs *et al.* 1976).